Journal of Quantitative Spectroscopy & Radiative Transfer 157 (2015) 54–70

Contents lists available at ScienceDirect

Journal of Quantitative Spectroscopy & Radiative Transfer

journal homepage: www.elsevier.com/locate/jqsrt

Size-dependent fluorescence of bioaerosols: Mathematical model using fluorescing and absorbing molecules in bacteria

Steven C. Hill [a,*], Chatt C. Williamson [a], David C. Doughty [a], Yong-Le Pan [a], Joshua L. Santarpia [b], Hanna H. Hill [c]

[a] US Army Research Laboratory, 2800 Powder Mill Road, Adelphi, MD 20783, USA
[b] Sandia National Laboratory, Albuquerque, NM, USA
[c] Silver Spring, MD 20904, USA

ARTICLE INFO

Article history:
Received 13 November 2014
Received in revised form
21 January 2015
Accepted 22 January 2015
Available online 2 February 2015

Keywords:
Fluorescence
Bioaerosols
Aerosol characterization
Light scattering

ABSTRACT

This paper uses a mathematical model of fluorescent biological particles composed of bacteria and/or proteins (mostly as in Hill et al., 2013 [23]) to investigate the size-dependence of the total fluorescence emitted in all directions. The model applies to particles which have negligible reabsorption of fluorescence within the particle. The specific particles modeled here are composed of ovalbumin and of a generic *Bacillus*. The particles need not be spherical, and in some cases need not be homogeneous. However, the results calculated in this paper are for spherical homogeneous particles. Light absorbing and fluorescing molecules included in the model are amino acids, nucleic acids, and several coenzymes. Here the excitation wavelength is 266 nm. The emission range, 300 to 370 nm, encompasses the fluorescence of tryptophan. The fluorescence cross section (C_F) is calculated and compared with one set of published measured values. We investigate power law (Ad^y) approximations to C_F, where d is diameter, and A and y are parameters adjusted to fit the data, and examine how y varies with d and composition, including the fraction as water. The particle's fluorescence efficiency ($Q_F = C_F$/geometric-cross-section) can be written for homogeneous particles as $Q_{abs}R_F$, where Q_{abs} is the absorption efficiency, and R_F, the fraction of the absorbed light emitted as fluorescence, is independent of size and shape. When Q_F is plotted vs. $m_i d$ or $m_i(m_r-1)d$, where $m=m_r+im_i$ is the complex refractive index, the plots for different fractions of water in the particle tend to overlap.

1. Introduction

Single-particle intrinsic fluorescence measurements are being investigated and used for detection and partial characterization of atmospheric aerosols [21,53,27,42, 38,60,32,59,29,49,40]. Fluorescence lidar is also being investigated for detection of atmospheric aerosols [17,57]. Polycyclic aromatic hydrocarbons and some other non-biological organic carbon compounds in atmospheric particles (e.g., smoke, soot) are also highly fluorescent [9]. However, the main interest in the intrinsic fluorescence of atmospheric aerosols [45,1] has been in detecting Primary Biological Aerosol Particles (PBAP). PBAP include fungi and pollens (and fragments of these), bacteria, algae, viruses, proteins, rotting wood, skin, etc. [19]. PBAP may be aerosolized by winds, abrasion, and injection. PBAP may

* Corresponding author.
E-mail address: steven.c.hill32.civ@mail.mil (S.C. Hill).

http://dx.doi.org/10.1016/j.jqsrt.2015.01.011

also be generated in the breakup of water, e.g., from raindrops impacting on surfaces, water waves breaking, bubbles in water bursting, persons sneezing or coughing [12], or flushing of toilets [28]. PBAP include re-aerosolized particles. Mass concentrations over vegetated regions are estimated to be $\sim 1\ \mu g/m^3$ for pollens and for fern spores; ~ 0.1 to $1\ \mu g/m^3$ for fungal spores and for plant debris; and $\sim 0.1\ \mu g/m^3$ for bacteria [19].

PBAP impact human health, agriculture, and the earth's climate. Pollens and fungal spores can cause allergies such as hay fever. Asthma can be exacerbated by pollens, fungal spores, bacteria, proteins from cats and dogs, and particles from cockroaches and dust mites. Airborne particles, primarily bacteria (e.g., tuberculosis) and viruses (e.g., norovirus and SARS [67]), are important means of disease transmission in humans [20] and other animals. Fungal spores and bacteria are major plant pathogens [2]. PBAP can scatter, absorb and re-emit atmospheric radiation. Therefore, the absorption and fluorescence properties of atmospheric pollen and fungal materials are relevant for understanding their effects on climate. PBAP can act as cloud condensation nuclei [58] and ice nuclei [66] and thereby affect cloud cover and precipitation patterns. “Uncertainties in aerosol forcing remain the dominant contributor to the overall uncertainty in net anthropogenic forcing” of global climate change ([56], p. 114; see also [15]).

Although intrinsic-fluorescence based instruments are relatively nonspecific and cannot identify specific bacteria, proteins, viruses, etc. [54,26,42,48], they are used to indicate increases in concentrations of certain bioaerosols and to indicate the need to collect and analyze air samples for identification of biothreats [54,26,48]. Such instruments are commercially available, e.g., the UV-APS (TSI), WIBS-4 (Droplet Measurement Technologies), Tac-Bio (Chemring), Bioscout (Environics Ltd.; see [50]) and IBAC (FLIR Technologies). See [29] for a history and discussion of fluorescence-based bioaerosol detectors.

In designing, developing, and optimizing methods to use such fluorescence-based instruments, questions arise regarding how the fluorescence of bioparticles varies with size, excitation and emission wavelengths, and particle composition. There is a need to develop test particles for such fluorescence-particle counters and spectrometers. These particles should be stable and have optical properties that can be used to verify if an instrument is operating properly. There are also questions regarding concentrations of fluorophores and other absorbing molecules, and the effects of dilution of these molecules by, e.g., water or salt, as can occur in laboratory generated particles [47], or in particles generated from breaking waves in the ocean, or in hygroscopic particles at moderate to high humidity. Such questions arise, in part, because it is often not possible to generate sufficiently narrow size-distributions of particles. Consequently, estimates of how the fluorescence varies with size are often needed in extracting fluorescence cross sections from a series of measurements and in calibrating instruments which measure particle fluorescence. Questions regarding the variation of fluorescence with particle size and composition are also relevant to understanding and modeling how the detectability and fluorescence of bioaerosols varies with exposure to components of the atmospheric environment such as ozone [51,43], reactive oxygenated species (ROS), nitrogen oxides, sunlight, etc., at various humidities [60]. Measurements of fluorescence of bioparticles, with and without exposure to sunlight, ozone, ROS, etc., are needed for models to be developed and validated. It is unlikely that sufficient resources would be available to test every case of interest, e.g., the type of bioparticle, the particle's specific composition, and how its reactions vary with sunlight, humidity, different types of ROS, etc. Therefore, there is interest in improving modeling capabilities for fluorescence of bioparticles and in attempting to find closure with measurements of: (a) particle fluorescence intensities and spectra; (b) compositions of bioparticles; (c) absorptivities and fluorescence cross sections of the relevant fluorophores and other absorbing molecules; (d) how fluorescence and refractive index of particles vary with water content; (e) how the relevant molecules are modified by sunlight, reactions with ROS, etc., at different water contents; (f) how the water content of different particles varies with humidity; and (g) how this relation between water content and humidity can vary as the molecules in the particles react with atmospheric constituents, with or without sunlight. The task is daunting. However, an even more daunting task would be to understand and predict the responses of different instruments to bioaerosols that have been exposed to various atmospheric conditions and constituents for various times, *without* modeling the fluorescence.

Hill et al. [25] attempted to address the dependence of bioaerosol fluorescence on size and composition. Two of the limitations of that work are: (a) it considered only one fluorophore and absorbing molecule, i.e., tryptophan; and (b) it compared the calculations only with measurements of relative fluorescence intensities. That is, only the shapes of the fluorescence-vs.-diameter curve could be compared with measurements. The amplitudes of the measured fluorescence had to be adjusted to fit with calculated values. The paper noted that, for very small or slightly absorbing particles, the fluorescence increases with d^3 for approximately spherical particles, but for large absorbing particles the fluorescence increases proportionally to a linear dimension squared (as the particle's geometric cross section). Since then, many researchers have asked how the fluorescence varies with particle size in the regions between these extremes. We have replied that the concentrations, absorptivities and fluorescence quantum yields of the relevant molecules are needed in order to calculate the total fluorescence cross sections.

Recently Hill et al. [23,24] published a set of fluorescence and absorption properties of the main fluorophores in bacteria, as well as concentrations of these molecules for two vegetative bacteria, a bacterial spore and two proteins. They assembled this information because it is required for calculating fluorescence cross sections of these bioparticles and because it helps in extracting size-dependent fluorescence cross sections from measured fluorescence data from particles of varying sizes.

In the present paper the concentrations and optical parameters are similar to those described previously [23,24], where the main modification is in some updated

densities and in also treating particles that are diluted with different fractions of water or mixed with salts. Also, in the present paper, the mathematical model is similar to that described [23,24], but with some additions: (a) some updated densities are used and expressions for the properties of spheres having various water fractions are given; (b) expressions for the fluorescence now explicitly indicate the non-radiative transfer of energy from one molecule to another; (c) an expression is given for the fluorescence cross section of particles composed of multiple homogeneous regions. Bacteria and proteins excited at the excitation wavelength used here (266 nm) more complex and interesting variations of fluorescence with size than do such particles excited at wavelengths longer than 300 nm where the absorption of light is much weaker.

2. Mathematical model of bioparticle fluorescence

The primary molecules used in the calculations by the mathematical model [23] are as follows: (1) the fluorophores tryptophan, tyrosine, NADH and NADPH, flavins, vitamins B_6 and K and their congeners, ubiquinone (and in bacterial spores, calcium dipicolinate (CaDPA)); (2) the absorbing but not fluorescing molecules phenylalanine and cystine in proteins, the nucleic acids (DNA, RNA, and small molecules such as adenosine diphosphate).

Primary assumptions and aspects of the mathematical model [23] which allow for a simplification in the calculations are as follows: (1) The absorbing and fluorescing molecules are randomly oriented in any region within the particle where the dimensions of the region are small compared to the wavelength but large compared to the dimensions of the fluorophores and absorbing moieties (e.g., adenosine in RNA). We think this is a useful assumption for the particles studied here. (2) The fluorescence calculated is the total fluorescence emitted from the particle. This assumption is probably adequate for comparing with instruments which collect light over a large (e.g., $>2\pi$ *sr*) solid angle, but will be of limited usefulness for instruments such as the WIBS [47] which measures fluorescence at different angles relative to the excitation beam. (3) The fluorescence emitted inside the particle is not reabsorbed in the particle. It exits from the particle. Thus the model is applicable only to cases where the reabsorption of fluorescence is sufficiently small so that its effects are negligible for the desired uses. The adequacy of this assumption for a given particle composition, size and wavelengths must be verified by calculation. This assumption is valid for the particle sizes and compositions for the illumination wavelengths discussed in this paper, but it is not likely to be useful for all bioaerosols, e.g., pollens, excited at all wavelengths.

In the mathematical model presented here the particle need not be spherical and homogeneous, and the illumination need not be with a plane wave, although we treat spherical homogeneous particles illuminated by a plane wave in our calculations and implementation. If a means is available for calculating the absorption in each homogeneous region of a nonspherical particle held in some orientation with respect to an incident wave, and if the assumptions stated above hold, then the approach presented here can be applied to that nonspherical inhomogeneous particle (see 2.2.5 below). Light scattering codes (e.g., [36], chap. 6) such as T-matrix methods, finite-difference time-domain (FDTD) methods, discrete dipole (DDA) or moment methods, are available for calculating scattering by highly complex particles. In doing such light scattering calculations for complex PBAP, the problem of finding an adequate light-scattering code may be less difficult than that of finding the concentrations of the relevant absorbing and fluorescing molecules in each region of the particle.

In the calculations presented here, the particle is homogenous and spherical, not because most bioaerosols are homogeneous and spherical, but because it is useful to first understand the main features of the simplest problem without being distracted by inhomogeneities or non-sphericities. It would be even more difficult to find reasonable approximations to the concentrations and parameters needed for calculations of inhomogeneous particles. Also, it is easiest to calculate results for the homogeneous sphere illuminated with a plane wave.

In the following description, the optical properties and parameters are wavelength dependent, but the subscripts and superscripts of the λ's (which represent the wavelengths in free space) are all suppressed to keep the notation from becoming unwieldy. The model naturally divides into two main topics: the optical properties of the materials comprising the bioaerosol, and the method of calculating fluorescence properties of homogeneous particles composed of these materials. The steps used are as follows.

2.1. Determine the optical properties of the bulk material comprising the particle

(2.1.1) Determine or estimate the concentrations (c^k) in mole/liter or in g/cm^3, where k indicates the kth substance. Although here we only calculate results for homogeneous particles, if the particle were to consist of a set of homogeneous regions, this determination would be repeated for each region. Aerosolized bacteria are often measured when they are relatively dry. The concentrations for some substances, e.g., DNA or proteins, are often specified in terms of the fraction of the dry weight. For other substances, the concentrations in the literature are for bacteria with the water content of a cell growing in a culture medium. The parameters used in the estimates: (a) densities, (b) mass fraction of water, (c) ratio of aqueous intracellular volume to cellular dry weight, and (d) volume per gram of some of the aqueous solutions, as discussed below.

(a) The density used for dry ovalbumin 1.28 g/cm^3 and for bovine serum albumin is 1.26 g/cm^3. The density used for wet vegetative cells is 1.098 g/cm^3 which was measured for *Bacillus anthracis* [14], and is similar to data of Kubitschek [30] for *Escherichia coli* and the fungus *Schizosaccromyces pombe*, and of Baldwin et al. [5] for *E. coli* at osmolarities similar those in standard phosphate buffered saline. The density used for dried vegetative cells is 1.43 g/cm^3 (a value in the range of those obtained by Delgado et al. [18] in their Fig. 2B).

Table 1
Chemical composition and imaginary component of refractive index for the *Bacillus* vegetative cells as used in this paper. The density used is 1.08. The real part of the refractive index is 1.59 at 266 nm, 1.58 at 280 nm and 1.548 at 355 nm. The absorption coefficient is in liter mole^{-1} cm^{-1} (except DNA/RNA is in cm^2/g, for DNA/RNA concentrations in g/cm^3). The mass fractions do not total to 100% because some molecules are counted twice (e.g., cystine is listed individually, but also is in total protein) and some non-absorbing materials are omitted to save space.

Material	Absorption coefficient	Fluorescence quantum yield	Bacillus vegetative cells		Ovalbumin	
			Mass fraction (g/g) dry weight (%)	Contribution to the imaginary refractive index at 266 nm	Mass fraction (g/g) dry weight (%)	Contribution to the imaginary refractive index at 266 nm
Tryptophan	4700	0.12	4.0	0.0064 (14.4%)	1.41%	0.002 (61.2%)
Tyrosine	900	0.003	3.5	0.0012 (2.7%)	3.74%	0.0011 (35.2%)
Phenylalanine	90	0.001	4.0	0.51×10^{-4} (0.11%)	7.97%	0.87×10^{-4} (2.7%)
Cystine	220	0	3.0	0.00017 (0.39%)	0.55%	0.28×10^{-4} (0.87%)
Protein			68.0	0.0078 (17.6%)	100%	0.0032 (100%)
DNA	23,300	0	3.0	0.0039 (8.7%)	0	0
RNA	3800	0	16.0	0.026 (58.1%)	0	0
Adenine(s) (not NAD/FAD)	14,000	0	0.2	0.00056 (1.3%)	0	0
Cytidine(s)	8900	0	0.23	0.00044 (0.99%)	0	0
Guanine(s)	11,000	0	0.48	0.0010 (2.3%)	0	0
Thymidine(s)	9900	0	0.37	0.0008 (1.8%)	0	0
Uridine(s)	9100	0	1.86	0.0036 (8.2%)	0	0
nucleic mono			3.1	0.0065 (14.5%)	0	0
NAD+NADP	5000	0	0.16	0.00025 (0.56%)	0	0
NADH+NADPH	31,800	0.04	0.062	0.3×10^{-4} (0.068%)	0	0
FMN+riboflavin	37,000	0.13	0.007	0.37×10^{-4} (0.08%)	0	0
FAD	1500	0.013	0.03	0.0001 (0.23%)	0	0
pyridoxal (PL)	1500	0.048	0.001	0.77×10^{-6} (0.002%)	0	0
PLP	1600	0.01	0.007	0.25×10^{-5} (0.005%)	0	0
Pyridoxamine	1600	0.11	0.001	0.34×10^{-6} (0.0007%)	0	0
PMP	1900	0.14	0.002	0.68×10^{-6} (0.002%)	0	0
Pyridoxine	14,800	0.07	0.001	0.8×10^{-6} (0.002%)	0	0
bound B_6 total		0.002	0.007	0.29×10^{-5} (0.006%)	0	0
Ubiquinone	14,000	0.002	0.0	0 (0%)	0	0
Ubiquinol	17,000	0.008	0.0	0 (0%)	0	0
Menaquinone	17,000	0.0026	0.027	0.72×10^{-4} (0.16%)	0	0
Menaquinol	4500	0	0.003	0.12×10^{-5} (0.0028%)	0	0
Total				0.045 (100%)	100%	0.0032 (100%)

The densities used for the spores, 1.17 g/cm^3 wet and 1.42 g/cm^3 dry, are in the ranges of those reported by Carrera et al. [14] for seven subspecies of *B. anthracis*. The overall range Carrera et al. [14] obtained for these eight subspecies as well as six other species of *Bacillus* was 1.15–1.223 g/cm^3 for the wet spores and 1.40–1.52 g/cm^3 for the dry spores (where the only dry *Bacillus* with density greater than 1.45 was *Bacillus subtilis*). For comparing with fluorescence measurements of different species of *Bacillus* the densities reported by Carrera et al. [14] for those species could be used instead of the value for the generic *Bacillus* used here. However, the densities of individual species of *Bacillus* reported in [14] are within 7% of the density used here for the generic *Bacillus*.

(b) The mass fraction of water used for wet cells is 0.7 ([18], in their Table 2). Higher fractions have been reported, e.g., 0.74, for *E. coli* ([31], p. 410), but these may have had more intercellular water in the wet samples.

(c) The ratio of the aqueous intracellular volume to cellular dry weight is 2.3 cm^3/g as used by Bennett et al. [7,8]. In using the density of 1.098 g/cm^3 given above for bacteria, and the aqueous intracellular volume of 2.3 cm^3/g, a volume of 1 cm^3 contains a dry mass of 0.3×1 cm^3 $\times$ 1.098 g/cm^3 = 0.33 g, which means the intracellular aqueous volume is 0.33 g $\times$ 2.3 cm^3/g = 0.76 cm^3. This value is used here in converting the concentrations of Bennett et al. [8] for nucleic acid monomers, flavins and other small molecules, which are given as moles/liter of the aqueous part of the cells, into moles per volume, or moles per mass, of the whole cell, which is needed for the average optical properties, which are best estimated using moles/liter or g/liter of the total volume. Therefore, the concentrations of the metabolites given by Bennett et al. [8] are converted here into units of moles/liter for the total cell by multiplying the concentrations of Bennett et al. [8] by 0.76.

(d) For particles of albumin combined with different amounts of water, the concentrations are estimated using approximations of the measured plots of volume per gram (V^m) (reciprocal of density) of the protein–water mixture vs. the fraction of water by mass (w), as shown in Sirotkin et al. [52] in parts A and B of their first figure. We approximate these curves as three linear segments:

$$V^m = V_0^m + w(V_s^m - V_0{}^m)/(w_{s1}) \quad \text{for } 0 < w < w_{s1},$$
$$V^m = V_s^m \quad \text{for } w_{s1} < w < w_{s2},$$
$$V^m = V_s^m + w(V_h^m - V_s^m)/(1 - w_{s2}) \quad \text{for } w_{s2} < w < 1.0,$$

where for ovalbumin $V_0^m=0.79$, $V_s^m=0.78$; for human serum albumin $V_0^m=0.795$, $V_s^m=0.77$; and in each case, $V_h^m=1.00296$, $w_{s1}=0.06$, and $w_{s2}=0.1$, at 25 °C.

(2.1.2) Determine or estimate the complex refractive index of the particle ($m=m_r+i\,m_i$) at each of the excitation and emission wavelengths. In another common notation, m_r is labeled n and m_i is labeled k. The m_i specifies the absorption per volume in a bulk material and the decrease in the intensity $I(z)$ of a plane wave as

$$I(z)/I_0=\exp(-4\pi m_i z/\lambda), \tag{1}$$

(see [10], p. 29, noting that their k is our m_i), which can be compared with the Beer–Lambert law, $I(z)/I_0=10^{-\varepsilon cz}$ ([34], p. 59–59, or [37], p. 76) where ε is the absorptivity (also known as the absorption coefficient or extinction coefficient), and c is the concentration. For the small molecules in this paper, ε is in liters/(mole cm), i.e., it is the molar absorption coefficient, and c is in moles/liter. Also, for proteins the ε is determined by summing the contributions from the amino acids. However, for DNA and RNA, the ε is in $cm^3/(g\,cm)$ and c is in g/cm^3. Comparison of these two expressions for $I(z)/I_0$, shows that m_i is related to ε and c as

$$m_i=\varepsilon c\lambda/(4\pi\log_{10}(e)) \tag{2}$$

When the material contains multiple species of molecules or macromolecules, the total m_i (i.e., ${}^Tm_i$) at any wavelength is

$${}^Tm_i=\sum {}^km_i=\lambda/(4\pi\log_{10}(e))\sum \varepsilon^k c^k, \tag{3}$$

where the contribution to the total m_i from the kth material is found as

$${}^km_i=\varepsilon^k c^k\lambda/(4\pi\log_{10}(e)) \tag{4}$$

where ε^k is the absorptivity of the kth material and c^k is the concentration. Estimating the m_i requires the concentrations per volume of the molecules that absorb light and the average absorptivities of each of the absorbing molecules. The absorptivities, concentrations, and ${}^km_i$ used in this paper are shown in Table 1, which are in most cases the same as those in [23,24].

The fraction of the total energy which is absorbed by the kth material is

$${}^km_i/{}^Tm_i. \tag{5}$$

The m_r of the dry *Bacillus* is assumed to be equal to that of *Erwinia herbicola* as reported by Arakawa et al. [4], i.e., 1.59 at 266 nm. The m_r of the dry ovalbumin at 266 nm is assumed to be 1.598 as reported by Arakawa et al. [3]. The m_r for particles containing water and solids is calculated as the average weighted by mass fractions of water and of the solids.

(2.1.3) Estimate the fluorescence quantum yields (φ_k) for each of the fluorophores (denoted by subscript k) as

φ_k=fluorescence emitted by the kth material/light absorbed by the kth material.

The φ_k used in this paper and the problems in estimating these are discussed in [23]. Because these φ_k are quantum yields the fluorescence emitted and the light absorbed are in units of photons and intensities are in photons/m^2. The properties of the fluorescing and absorbing molecules and the concentrations of molecules and the calculated imaginary refractive indices for *B. subtilis* vegetative cells and ovalbumin at 266 nm as used here are shown in Table 1. As in [23], only one value is used for the φ of tryptophan. In most cases we will have no further information about the φ of tryptophan in any specific bacteria or protein and will be forced to use some best estimate value. By using only one value for the φ of tryptophan here, we are using the approach we will most commonly be forced to take. However, if values of φ for tryptophan or other molecules in specific proteins or other bioparticles are known, they should be used in comparing with measurements of those bioparticles. For example, the reported value for the φ for tryptophan in ovalbumin is approximately 0.24 [35], which is approximately twice as large as the value used here. However, all the findings about the *size dependence of fluorescence* reported here, are unaffected by the specific value of φ used for tryptophan because tryptophan is the only significant fluorophore.

In the bacteria investigated here at 266 nm, the absorption is dominated by nucleic acids (DNA, RNA and free nucleotides and nucleosides) and aromatic amino acids. In ovalbumin, the absorption is dominated by aromatic amino acids. Tryptophan strongly dominates the fluorescence in both particles. The absorption efficiencies and concentrations for a variety of molecules that contribute very little to the 300–360-nm fluorescence excited at 266 nm are included in Table 1 because: (a) they are included in the calculation of absorbance at 266 nm (although their contribution may be negligible at this wavelength), and (b) they are also used in verifying that the reabsorption of the fluorescence emitted by tryptophan is small (see [23] for the relevant absorptivities at 339 nm).

2.2. Calculate the fluorescence cross section and particle fluorescence efficiency

(2.2.1) Calculate the absorption cross section (C_{abs}) of the particle and the absorption efficiency (Q_{abs}), i.e., C_{abs} divided by the geometric cross section of the particle for its particular orientation in the illumination beam. These can be calculated for highly complex and inhomogeneous particles or agglomerates using a variety of methods ([36] chap. 6). For the spherical particles studied here,

$$Q_{abs}=C_{abs}/\pi r^2, \tag{6}$$

where r is the radius, and Q_{abs} is calculated here using the codes in [6].

(2.2.2)Calculate the fraction of C_{abs} attributable to the kth fluorophore as

$${}^kC_{abs}=C_{abs}\,{}^km_i/{}^Tm_i, \tag{7}$$

when there is no non-radiative energy transfer from one molecule to another. To take into account the non-radiative transfer of energy from the jth molecule to the kth fluorophores (e.g., from tyrosine to tryptophan) the fraction of the C_{abs} attributable to the kth fluorophore can be written as,

$${}^kC_{abs}=C_{abs}\sum\nolimits_j \eta_{kj}\left(c^k,c^j\right)^j m_i/{}^Tm_i, \tag{8}$$

where $\eta_{kj}(c^k,c^j)$ is the fraction of the energy absorbed by the jth material that is transferred nonradiatively to the

kth material. This transferred energy can be re-emitted by the kth component with the usual quantum yield, φ_k. When $j=k$, then $\eta_{kj}(c^k,c^j)=1$. When $j\neq k$ then $\eta_{kj}(c^k,c^j)$ is usually zero. To keep ${}^Tm_i$ and C_{abs} constant, the energy transferred to the kth material must equal the energy lost by the jth material, and so $\eta_{kj}(c^j,c^k)=-\eta_{kj}(c^k,c^j)$. This fraction $\eta_{kj}(c^k,c^j)$ depends upon the concentrations of the molecules, the spacings between them, and their orientations relative to each other.

For the calculations in this paper, where the excitation wavelength is 266 nm, the most significant off-axis η_{kj} is the one specifying the fraction of energy absorbed by tyrosine that is transferred to tryptophan. Here this fraction is assumed to be 0.3 in an attempt to be consistent with the data and discussion of [35, p. 430–437]. Because the tyrosine concentration can exceed that of tryptophan in some proteins by factors of more than 10, this transfer of energy from tyrosine to tryptophan can significantly affect the fluorescence. Unfortunately, we do not have sufficient information to estimate an average $\eta_{kj}(c^k,c^j)$ for other important pairs of molecules which transfer energy non-radiatively, e.g., tryptophan to NADH, or tryptophan to pyridoxamine phosphate (PMP) [55]. However, the concentrations of these other molecules are sufficiently low compared to those of tryptophan and tyrosine that for the particles studied here excited at 266 nm, and for the emission wavelength range used (where tryptophan fluorescence dominates), the effect on the fluorescence should be small relative to the uncertainty in fluorescence quantum yield for tryptophan in the bacteria.

(2.2.3) Calculate the total fluorescence cross section (${}^TC_F$), defined as

$${}^TC_F = I_F/I_{inc}, \tag{9}$$

where I_F is the total fluorescence emitted into all angles when the particle is illuminated by a plane wave with intensity I_{inc}. This I_F and I_{inc} here are in photons/m^2 because the φ_k are quantum yields. For I_F and I_{inc} in W/m^2 the φ_k are fluorescence yields which are the fluorescence quantum yields reduced by the ratio of the average fluorescence frequency to the incident frequency. For 266 nm excitation an average emission wavelength of 330 nm, which is reasonable for tryptophan, the fluorescence yield is approximately 266 nm/330 nm, or 0.8, times the fluorescence quantum yield.

This ${}^TC_F$ is calculated as

$${}^TC_F = \sum\nolimits_k {}^kC_F \tag{10}$$

where the contribution of the kth material to the total fluorescence cross section for the particle is

$${}^kC_F = \varphi_k C_{abs} \sum\nolimits_j \eta_{kj}\left(c^k,c^j\right){}^jm_i/{}^Tm_i, \tag{11}$$

and so the fluorescence cross section is

$$C_F = C_{abs}\sum_k \phi_k \sum_j \eta_{kj}\,{}^jm_i/{}^Tm_i \tag{12}$$

A relation that can be useful in understanding the size-dependent fluorescence of particles is obtained by rewriting Eq. (12) as,

$$C_F = C_{abs}R_F \tag{13}$$

where

$$R_F = \sum_k \phi_k \sum_j \eta_{kj}\,{}^jm_i/{}^Tm_i, \tag{14}$$

is the ratio of the energy emitted as fluorescence to the energy absorbed. Therefore, C_F in Eq. (13) is seen to be the product of R_F, which is independent of the size and shape and depends only upon the absorbers and fluorophores in the material, and C_{abs}, which depends upon the particle size, shape, and ${}^Tm_i$. The C_{abs} is independent of the fluorescence quantum yields and of the particular set of materials which have that ${}^Tm_i$.

(2.2.4) Calculate the particle fluorescence efficiency as ${}^TC_F$ normalized by the geometric cross section, which for a sphere is,

$$Q_F = {}^TC_F/(\pi r^2). \tag{15}$$

(2.2.5) For a particle composed of N homogeneous regions illuminated by a plane wave of intensity I_{inc}, the ${}^TC_F$ is

$${}^TC_F = I_F/I_{inc}, \tag{16}$$

where

$$I_F = \sum\nolimits_k {}^kR_F W_k, \tag{17}$$

and W_k is the energy absorbed in the kth region, and ${}^kR_F$ is the ratio of the energy emitted as fluorescence to the energy absorbed for the kth region.

(2.2.6) Verify that the absorption at the emission (fluorescence) wavelength is sufficiently small to be ignored. To do this, calculate the penetration depth (δ_{fl}) for a plane wave in a bulk material using λ_{fl} (the free space wavelength of the fluorescence), the m_i at λ_{fl}, and Eq. (1), as:

$$\delta_{fl} = \lambda_{fl}/(4\pi m_i). \tag{18}$$

Then verify that $\exp(-4r/\delta_{fl}) > 0.9$, i.e., a plane wave can travel a distance of two particle diameters and decrease less than 10% in amplitude. A more thorough analysis of the fluorescence that exits the sphere (e.g., [16,65]) is complex and time consuming. In a ray-trace approximation of the fluorescence, each time the ray meets the sphere surface it either exits the sphere or reflects internally. When $\delta_{fl}=4r=2$ diameters, all rays remaining in the particle after traveling a distance of δ_{fl} will have reflected from the surface of the particle at least two times, and most of the remaining rays will have reflected least four times. In using ray optics to model the intensity inside a large droplet, Velesco et al. [63,64], noted “no discernible differences between the results of three or eight internal reflections.” In a homogenous perfect sphere some of the rays will be trapped inside and not exit, but in full wave solutions to Maxwell's equations, the light has a finite lifetime. Also, real bioaerosols are typically not perfectly smooth or totally homogeneous, and so even in the ray approximation the light is not completely trapped by repeated total reflection. There are reasons to think that the use of a spherical shape in the model will not cause discrepancies that are large compared to the variability in reported measurements of fluorescence cross sections: (1) The total fluorescence cross section is proportional to the absorption by particles

when there is no reabsorption of fluorescence. Measured fluorescence cross sections are typically for averages of many particles where there seems to be no reason to assume these particles have a preferred orientation. (2) Calculations of randomly oriented spheroids with an aspect ratio of 1.4 indicate that the absorption cross section is within about 5% of the absorption cross sections of equal surface area spheres with refractive index $1.53+i$ 0.008 ([36], p. 294–295). This result holds for both prolate and oblate spheroids. However, the effect is as large as 5% only for particles with d/λ much smaller than those studied here. For aspect ratios of 2.0, the results are within about 17% in the worst case, which again occurs for particles much smaller than those studied here.

In cases where m_i is low but not zero, morphology dependent resonances, also known as whispering gallery mode resonances, may be noted in calculations of C_{abs} of spherical or spheroidal particles. Absorption of light at resonance wavelengths can require careful attention in cases where the m_i is very small [22]. However, the amplitudes of such resonances tend to be strongly reduced in particles which have non-smooth surfaces or which absorb light as well as do the bioparticles illuminated at 266 nm modeled here. Most biological particles are sufficiently nonspherical and/or inhomogeneous to reduce the amplitudes of these resonances and leave relatively smooth curves of absorption vs. size. An example of a bioparticle that is homogeneous and spherical is one composed of albumin and sufficient water to dissolve all the albumin. In some cases in this paper the resonances appear more prominent than they would be even for spherical particles because the lines used in the plots are thicker that the resonance linewidths.

3. Results and discussion

Reabsorption of the fluorescence within the particle was verified to be small for the cases modeled here, as outlined in 2.2.5 and as follows. The emission wavelength was assumed to be 0.339 μm, and the optical parameters for this wavelength were as in [23]. Assuming all the emission is at 0.339 μm leads to an overestimation of the absorption because much of the fluorescence is at wavelengths that are absorbed less. This overestimation is adequate for our goal of keeping within a range where reabsorption is negligible. Of the particles considered here, the ones with the highest reabsorption have the composition of 99% *Bacillus* and 1% water. The largest particles with this composition have $d=12$ μm. For this worst case, a plane wave could travel two particle diameters (24 μm) and only decrease in intensity by 7.3%. That decrease is negligible compared to uncertainties in particle composition and any single-particle fluorescence measurements of which we are aware. A wave could travel 26 of these 12-μm particle diameters before its intensity decreases to $1/e$. The large majority of the fluorescence would exit the particle after traveling distances smaller than two particle diameters. Therefore the assumption of negligible reabsorption should be adequate for the cases described below.

3.1. Fluorescence vs. diameter: calculated cross sections and measured relative amplitudes

After we understood that we had underestimated the importance of absorbing and fluorescing molecules other than tryptophan in *B. subtilis*, we wondered why our previous plots of fluorescence vs. size compared as well as they did. These had been plotted for measured relative fluorescence of *B. subtilis* and for calculated fluorescence of homogenous particles containing tryptophan [25].

Fig. 1 shows the measured fluorescence (relative intensity as described in [25]) (scale on the right), and calculated fluorescence cross section (scale on the left), both as a function of particle diameter. The measured data (from [25]) are the same in each panel. The values were measure as follows: (a) *B. subtilis* was suspended in water; (b) the suspension was aerosolized using an ink jet aerosol generator; (c) the generated particles were illuminated with a pulsed laser operating at 266 nm which was triggered to fire when a particle was detected (i.e., when the light it scattered from two crossed-beam diode lasers was detected); (d) the fluorescence was collected with a large solid-angle lens centered at 90° from the direction of the illumination beam; and (e) the intensity was recorded using an intensified CCD camera. In each panel in Fig. 1, the scale of the calculated fluorescence was adjusted to give similar amplitudes to the measured and calculated curves.

Several features are apparent in Fig. 1. First, the calculated curves appear to be decent fits to the measured data, good enough to give the impression that the model parameters are not terribly far from the actual values. However, in the calculations in Fig. 1(a) tryptophan is the only light-absorbing molecule ($m_i=0.0064$), while in the calculations of Fig. 1(b), only 14% of the light is absorbed by tryptophan ($m_i=0.045$), as in Table 1. Although the amplitude of the calculated C_F varies by a factor of almost six between Fig. 1(a) and (b), the shapes of the calculated curves do not change dramatically. That suggests that without measurements of the absolute C_F vs. size, comparisons such as those shown here may lack the power to distinguish between quite different assumptions about particle composition, at least when plotted in this way.

3.2. Log–log plots of particle fluorescence vs. size: calculated and measured

Fig. 2 shows the same data as in Fig. 1, but plotted as log (C_F) vs. log(d). As in Fig. 1, even though the absolute magnitudes of the two calculated curves differ by a factor of seven, the shapes of the calculated curves appear to be decent fits to the measured data.

The approximate linearity of the log(C_F) vs. log(d) plots in Fig. 2 motivates questions regarding how linear such plots would be for a larger range of particle sizes and compositions. Therefore, in Fig. 3 the mass fraction of water in a *Bacillus* particle is varied, and the range of d is extended to include particles smaller than 100 nm. The 0.1 μm diameter particles in Fig. 3 have fluorescence approximately proportional to concentration, e.g., particles with 98% solids have approximately 10 times the fluorescence of the particles with 10% solids. On the other hand, the 10-μm diameter particles with 98% solids have only approximately 10% more

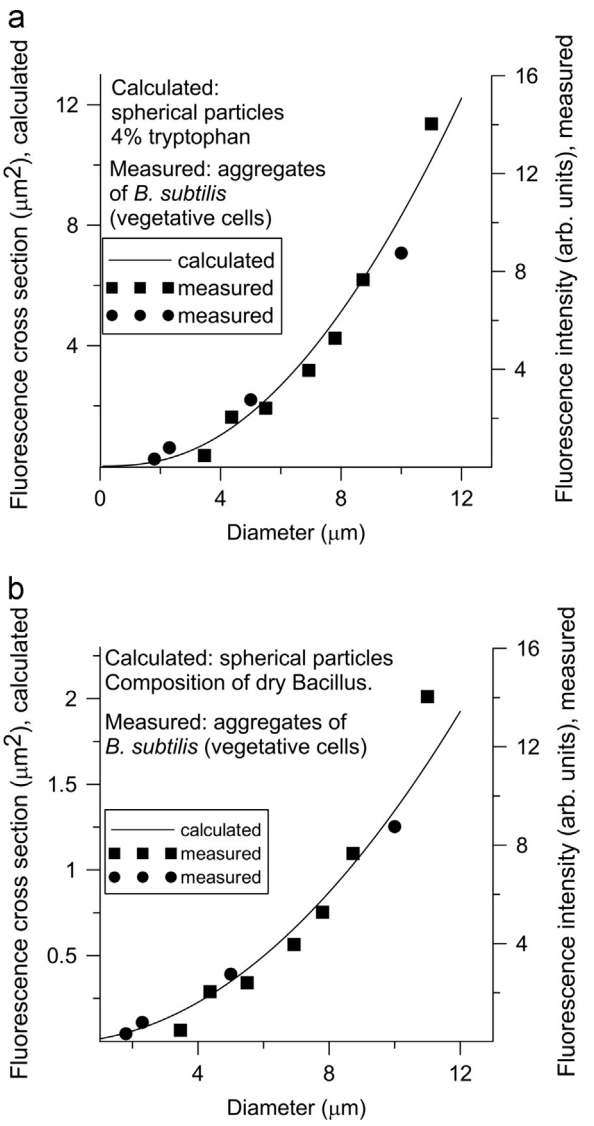

Fig. 1. Calculated fluorescence cross sections (solid line, left scale) and measured fluorescence intensity (circles and squares, right scale), each vs. particle diameter. For each calculated curve, the concentration of tryptophan in the solids is as in Table 1, and the fluorescence yield of tryptophan is 0.12. In (a) no absorbing or fluorescing molecules other than tryptophan are included, the refractive index is $1.59+i\ 0.0064$, and the scale on the left is from 0 to 12. In (b) all the molecules listed in Table 1 are included, 30% of the energy absorbed by tyrosine is transferred non-radiatively to tryptophan, and the labels on the scale on the left are from 0 to 2.

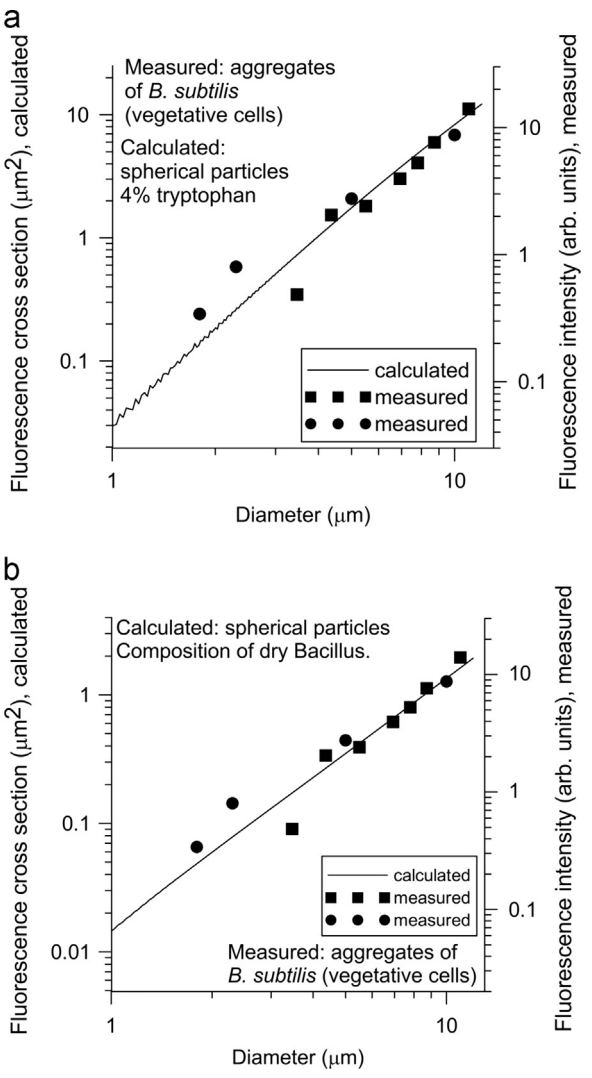

Fig. 2. Log–log plots of calculated fluorescence cross sections (solid line, left scale) and measured fluorescence intensity (circles and squares, right scale) each vs. particle diameter. In (a) no absorbing or fluorescing molecules other than tryptophan are included. In (b) all the molecules listed in Table 1 are included.

fluorescence than the 10-μm particles with 10% solids. That is, for $d=10\ \mu m$, and for the concentrations shown, the fluorescence is almost independent of concentration. This type of observation suggests that some care is needed in interpreting measurements. At intermediate sizes, e.g., 1 μm diameter, the particles with the lowest concentrations of solids still have fluorescence approximately proportional to concentration of solids; however, particles with higher concentrations of solids have fluorescence that increases less rapidly than concentration does. These differences suggest a need for further examination.

3.3. *Particle fluorescence efficiency vs. size: measured and calculated*

Fig. 4 illustrates the calculated particle fluorescence efficiencies (Q_F) plotted vs. d. The shape of each curve is determined by the shape of its absorption efficiency curve (Q_{abs}). In contrast to Figs. 1 and 2, there is a larger difference between the shapes of the two calculated curves in (a) and (b) of Fig. 3. This difference occurs in part because the d^2 variation, which is removed in Fig. 3, dominates the variation with d in Figs. 1 and 2. The measured values of Q_F appear to be much noisier, especially in the 2–4 μm diameter range, where the measured amplitudes are smallest. The clear differences between these calculated Q_F curves, and the known usefulness of Q_{abs} in light-scattering studies, suggest further examination of Q_F for better understanding variations in particle fluorescence with size, and for possibly extracting

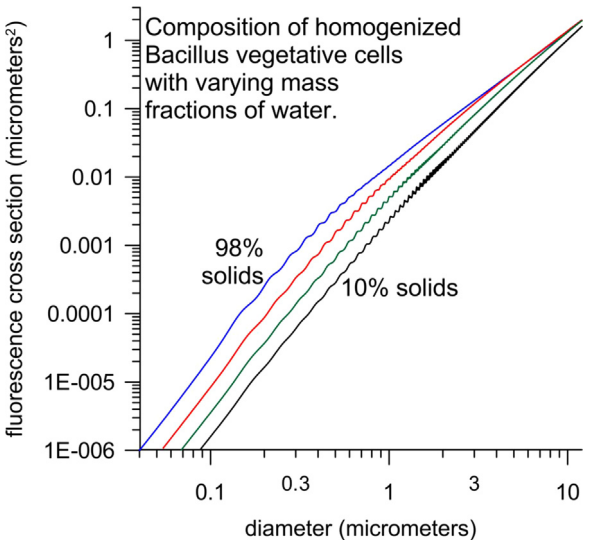

Fig. 3. Calculated fluorescence cross sections for spherical particles with the refractive index of homogenized *Bacillus* vegetative cells mixed with different mass fractions of water. The mass fractions of the solids are 98%, 46%, 21% and 10%, in the curves shown from left to right.

information about particle composition, e.g., variations in water content which might occur because of variations in humidity [43].

Fig. 5(a–c) indicates the dependence of fluorescence efficiency on diameter and on water content, for *Bacillus* vegetative cells (Fig. 5(a), properties given in Table 1), *Bacillus* vegetative cells with no absorbing or fluorescing molecules other than tryptophan (Fig. 5(b)), and ovalbumin (Fig. 5(c)). In Fig. 5(a) the particles with smallest concentrations of solids (10% and 21%) have fluorescence approximately proportional to concentration at the smallest sizes. However, for larger sizes the fluorescence efficiency reaches a maximum value of approximately 0.018 for particles having diameters of 0.6 μm at 98% solids, 4 μm at 46% solids and 9 μm at 21% solids. A zeroth order assumption might be that for a particles of a given size, those particles with more bacterial solids will have significantly more fluorescence than particles with only 50% or 22% of solids. However, Fig. 5 illustrates that this is not the case. In Fig. 5(a), the 8 μm diameter spheres have particle fluorescence efficiencies within a few percent of 0.018 whether they have 98% solids, 46% solids or 21% solids. Even the 4 μm diameter spheres with 46% solids have fluorescence within 5% of the spheres with 98% solids. The fluorescence cross section per volume decreases as d increases.

A difference between Fig. 5(a) and (b) is that in (b) the fluorescence vs. size curves are all stretched toward larger diameters (to the right) which is consistent with the shape of the Q_F vs d curve being determined by that of Q_{abs}. In Fig. 5(b) and (c), the Q_F depends strongly on the water content at all diameters from 0.1 to 12 μm. Also, the amplitudes of resonances, and the d at which these resonances occur, decrease as the content of the absorbing solids increases. These curves suggest the importance of knowing the percentages of non-fluorescing and non-absorbing materials (e.g., water, salts, dextrose), if any, that are mixed with the organisms and/or proteins in

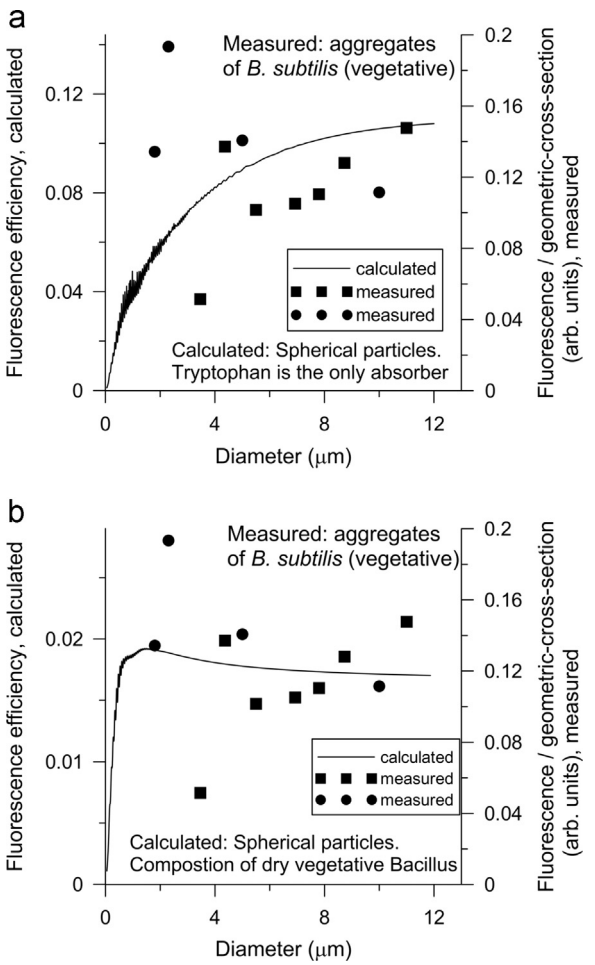

Fig. 4. The calculated particle fluorescence efficiency (Q_F) plotted vs. d. The solid lines are calculated. The solid squares and circles are measured values (i.e., measured fluorescence divided by $\pi d^2/4$). In (a) the only absorbing and fluorescing molecule is tryptophan and $m=1.585+i\ 0.0063$. In (b) the composition of the calculated particles is that of *Bacillus*, $m=1.585+i\ 0.045$.

particles. Note in Fig. 5(c) that if the fluorescence quantum efficiency used for tryptophan molecules in ovalbumin was the actual value for ovalbumin, e.g., 0.24 as reported in Longworth [35], the scale on the vertical axis would be approximately two times higher. Then dry 12 μm particles of ovalbumin would have C_F and Q_F approximately 14 times that of the dry Bacillus.

No results for excitation at wavelengths other than 266 nm are shown here. However, [23], (Tables 2–4) indicate that, at 355 nm excitation, $m_i=0.72\times10^{-4}$ for *E. coli*, $m_i=0.76\times10^{-4}$ for vegetative *Bacillus*, and 0.00039 for *Bacillus* spores. Also, the absorptivities in [23,1] indicate that for excitation at 325, 339 or 450 nm, the m_i for *E. coli* or vegetative *Bacillus* will not exceed $m_i=0.8\times10^{-4}$. These m_i are approximately 1/3rd of the lowest m_i in any plot in Fig. 5, i.e., the 0.00026 in Fig. 5(c). Therefore, for 325, 339 or 450 nm excitation of these clean bacteria, the Q_F will increase approximately linearly with d when d is less than 12 μm. This relation may not apply if the bacteria have too many impurities [33,41].

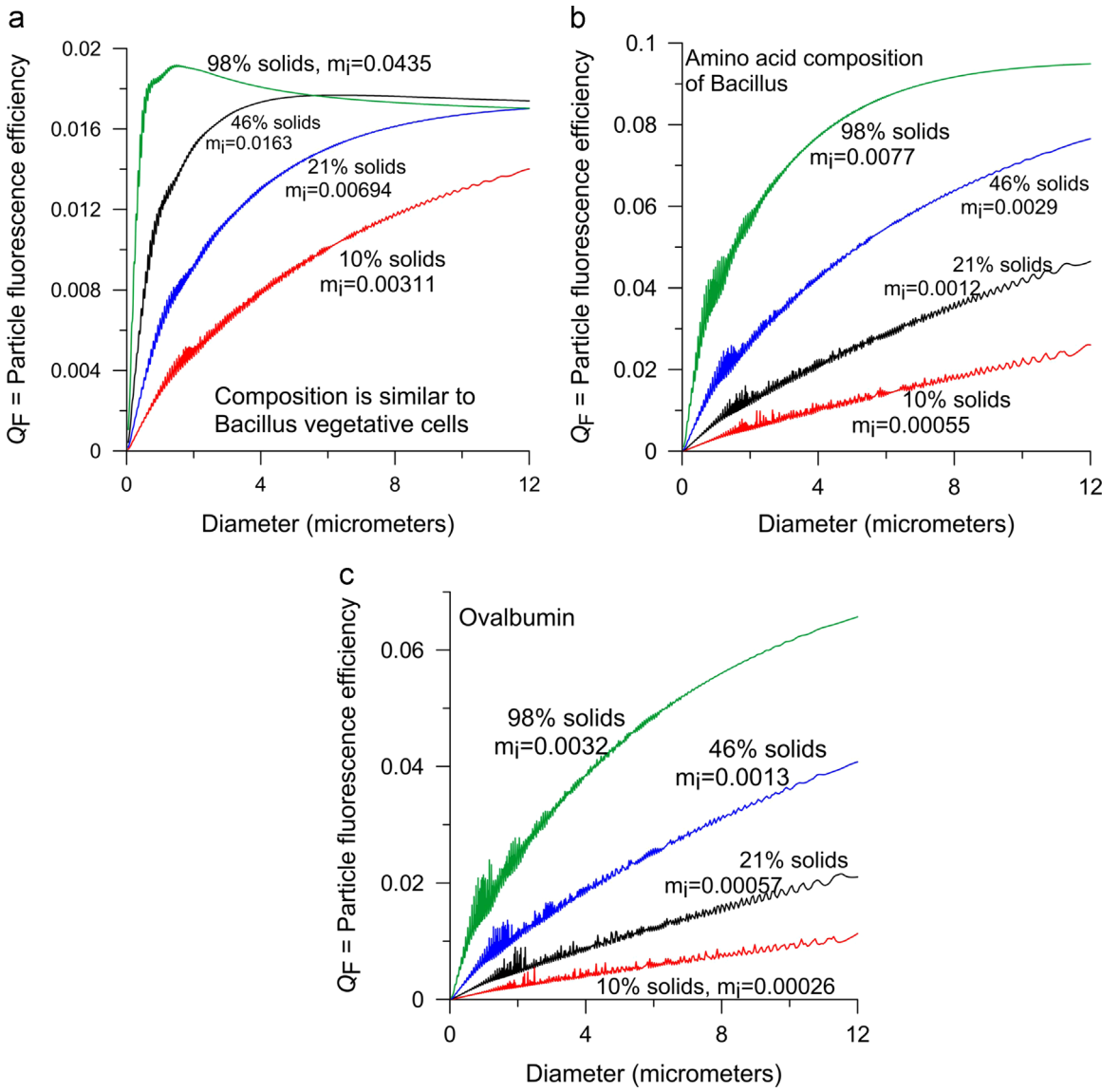

Fig. 5. Particle fluorescence efficiency vs. diameter for homogeneous particles having different percentages of solids in water. The solids have the following compositions: (a) *Bacillus* vegetative cells; (b) the amino acid composition of *Bacillus* vegetative cells but with no other absorbing or fluorescing molecules; and (c) ovalbumin. The curves are labeled by the percentage of solids in water.

In Fig. 6(a) the Q_F are plotted vs. the $d \times m_i$ (upper axis) and vs. a dimensionless diameter (d/δ) on the (lower axis). Here

$$\delta = \lambda/4\pi m_i$$

is the penetration depth, i.e., the distance a plane wave travels in a medium before it decreases to $1/e$ of its starting intensity. The curves of the fluorescence vs. d/δ or vs. $d \times m_i$ in Fig. 6(a) are much closer to overlapping than are the curves in Fig. 5. That overlap occurs primarily because, for these absorbing particles, d/δ is the relevant dimensionless particle diameter, i.e., the diameter as the number of $1/e$ distances. In Fig. 6(a) the real part of the refractive index varies with the fraction of water, as described in section 2.1.2. However, the value of d/δ at which each curve reaches its maximum or point of leveling increases as the fraction of solids decreases.

In Fig. 6(b) the Q_F are plotted vs. $(m_r-1)d/\delta$ on the lower axis, and vs. $m_i(m_r-1)d$ on the upper axis. In Fig. 6 (b) the curves first reach their maxima at approximately the same value, when $(m_r-1)d/\delta$ is approximately 2. The factor (m_r-1) is used following Van de Hulst [61], (chap. 11) and Penndorf ([44], Fig. 2) in their use of a normalized size parameter, that is, the phase shift parameter, $\rho = (m_r-1)\pi d/\lambda$, to overlay the curves of the scattering efficiency (Q_{sca}) calculated for different m_r.

In Fig. 6(c) the axes are the same as in Fig. 6(b), but $m_r = 1.585$ for all cases. This m_r should be an appropriate estimate for bioparticles mixed with a NaCl ($m_r = 1.63$ at 266 nm) and an appropriate amount of another salt or some carbohydrate. Not all the curves overlap even when

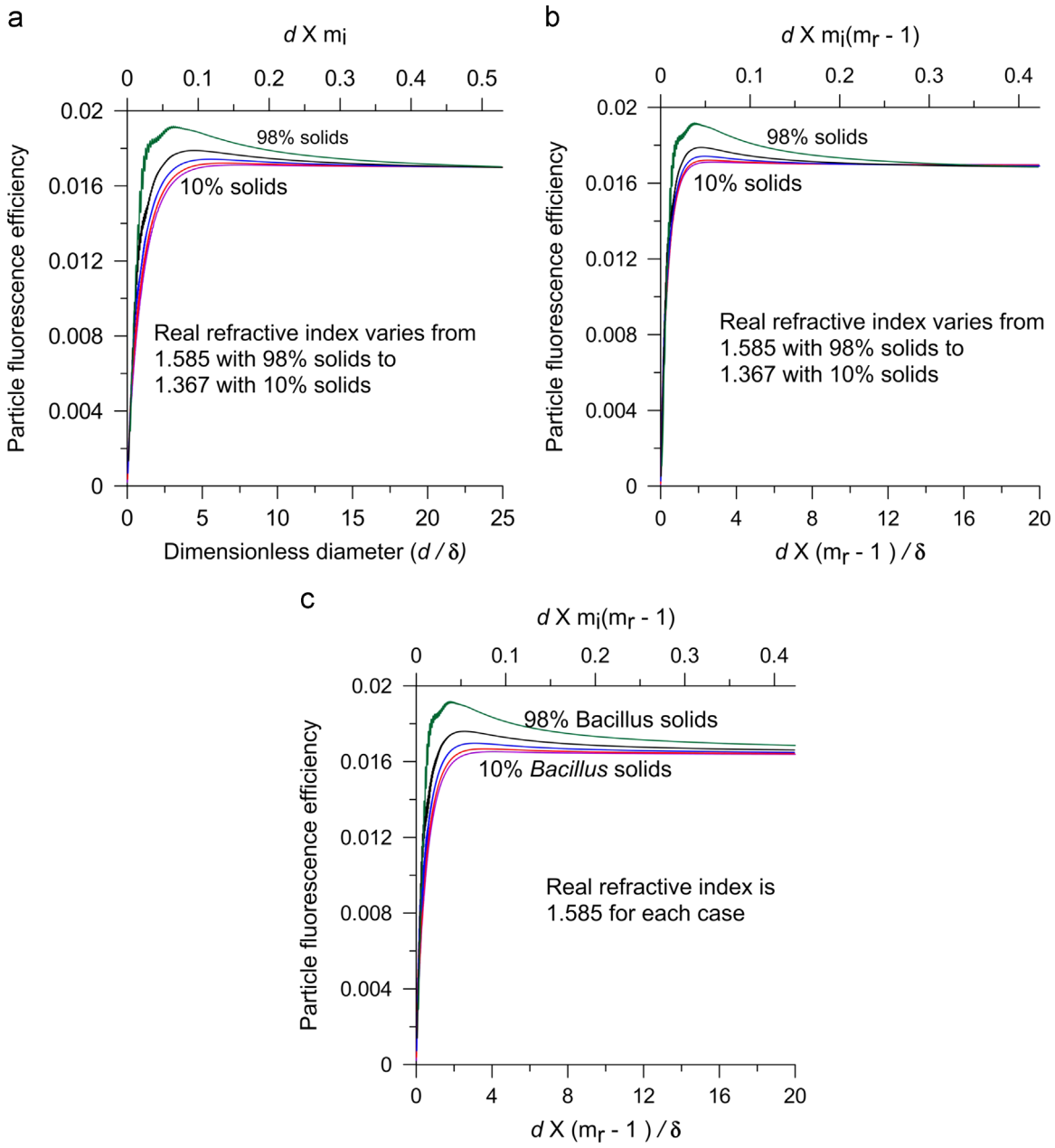

Fig. 6. Particle fluorescence efficiency (Q_F) for *Bacillus* with various fractions of water. In (a) plotted vs. d/δ (lower axis) and $d \times m_i$ (upper axis). In (b) and (c) plotted vs. $(m_r-1)d/\delta$ (lower axis) and $m_i(m_r-1)d$ (upper axis). In (a) and (b) the m for each curve from top to bottom is, $1.585+i\ 0.0435$, $1.4797+i\ 0.0205$, $1.4197+i\ 0.0105$, $1.3859+i\ 0.0057$ and $1.367+i\ 0.0031$. In (c) $m_r=1.585$ in all cases and the m_i are as in (a) and (b).

$d/\delta=20$, but at sufficiently large d they do overlap (not shown).

3.4. *Internal intensity distributions and relations to d/δ, angular scattering and inhomogeneities*

The internal intensity distributions shown in Fig. 7 help in visualizing why the fluorescence cross sections are proportional to volume when the combination of particle size and concentration of absorbing molecules are small, but are proportional to surface area when the size and concentrations of absorbing molecules are higher. For larger particles (Fig. 7(b)), the high intensity in the sphere is near the illuminated surface and so the fluorescence increases approximately as surface area or d^2. For smaller particles (Fig. 7(a)), the high intensity is far more uniform over the volume of the particle and energy is absorbed throughout most of the volume. In cases where d/δ is greater than approximately 2 or 3, the

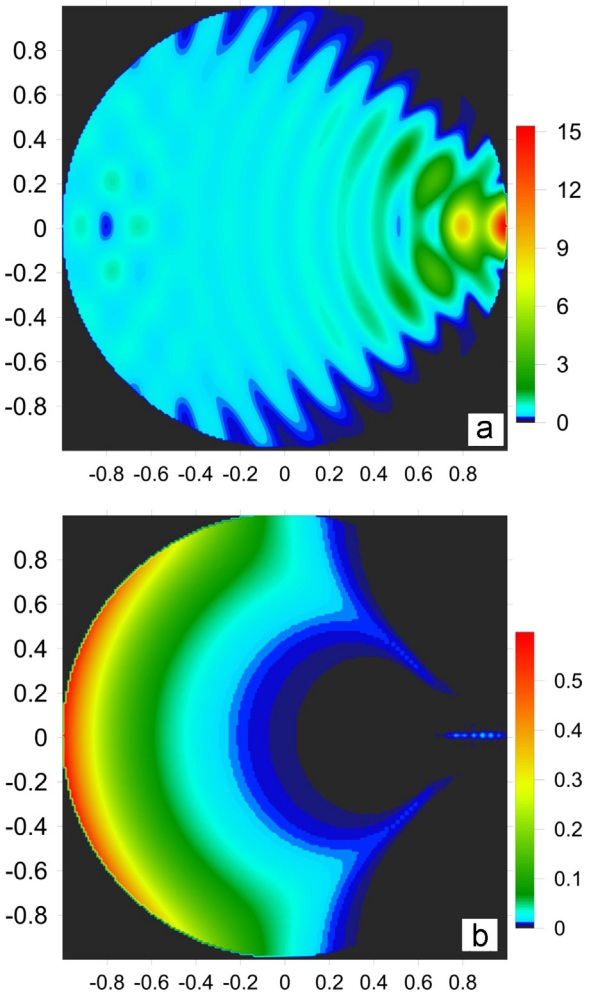

Fig. 7. Distribution of intensity (illustrated in false color) inside a homogeneous sphere with the complex refractive index of dry *Bacillus* vegetative cells, calculated using Barber and Hill [6]. Shown is a cross section through the center of the sphere. The sphere is illuminated by a plane wave incident from the left. (a) $d=1$ μm and $d/\delta=2.1$. (b) $d=6$ μm and $d/\delta=12.7$. The colored bars on the right of each figure indicate that the peak intensity in the sphere in (a) is approximately 15/0.6, or 25 times larger. (For interpretation of the references to color in this figure legend, the reader is referred to the web version of this article.)

dominant features of the internal intensity distributions should be similar for particles with the same d/δ.

In the model described here, only the total fluorescence is treated, i.e., the angular distribution of the fluorescence from particles is ignored. Backward enhancement of the fluorescence from particles has been reported in fluorescence calculated and measured for spheres [13], and in fluorescence measured for nonspheres [39]. The backward enhanced fluorescence is explained based on reciprocity, which applies when there is a strong similarity between the internal intensity distribution (as in Fig. 7(a)) and the regions in the sphere from which light is collected in the backward direction. The internal intensity distribution in the 1-μm sphere in Fig. 7(a) is similar to those in the previous calculations [13]. Even so, it is not likely to have much backward enhancement of the fluorescence because d/δ is larger than in the previous calculations and is in the transition region between large and small values. On the other hand, the intensity distribution in the 6-μm sphere in Fig. 7(b) is very different from that in the previous calculations in that the energy absorbed is largest on the illuminated side. The fluorescence from the model sphere in Fig. 7(b) is not one for which reciprocity is expected to be applicable because d/δ is relatively large for the incident wave (266 nm). However, the d/δ_{flu} for the fluorescence is much smaller than one, and so the shape of the distribution for collection of the light is much more similar to that in Fig. 7(a). At excitation wavelengths longer than 300 nm the m_i of proteins and most bacteria are much smaller than is the m_i of either the *Bacillus* or albumin excited at 266 nm illustrated here [23]. Therefore, d/δ should be less than 1 for particles composed of clean bacteria or proteins having d less than 15 when excited at wavelengths >300 nm.

3.5. Slope of log(C_F) vs. log(d) for different particle diameter and fractions of water

The slopes of the curves in the log(C_F) vs. log(d) vary with the particle composition and size (Fig. 3). These variations in the slopes are also seen in Fig. 8 which shows these slopes plotted against the diameter for *Bacillus* (Fig. 8(a)) and albumin (Fig. 8(b)) particles. For each of these figures the fraction of solids in water varies from 10% to 98%. In Fig. 8 these slopes approach 2.8 to 3 (i.e., approach a proportionality to volume) for the combinations of smallest diameter and lowest percentage of solids. The slopes approach two (proportional to cross section) for particles with 98% solids with the composition of *Bacillus*, even when the particle diameters are as small as 2. On the other hand, for particles that are only 10% or 18% albumin in water, the slope approaches 2.8 and decreases very slowly if not negligibly in the 1 to 15 μm diameter range shown.

Fig. 9 illustrates the slopes of log(C_F) vs. log(d) plotted vs. mass fraction of solids in water. The fraction of solids in water varies from 10% to 98%. Fig. 9, in effect, selects several diameters from Fig. 8 and for each plots the slopes of log(C_F) vs. log(d) against the fraction of solids in the particle.

Calculations such as those shown in Figs. 8 and 9 should be useful for estimating or verifying the content of water, salts, or other nonfluorescent materials in the particles at the time they are measured.

3.6. Fluorescence-divided-by-Ad^y vs. diameter for different values of A and y

A motivation for this work has been the need to estimate how fluorescence varies with size and composition in order to estimate particle-size-independent optical properties from single particle measurements over a range of particle sizes. In Fig. 10 the calculated fluorescence vs size for different solid fractions of *Bacillus* in water is divided by the best fit estimate (florescence varies as Ad^y). For each curve, the best fit values A and y, for approximating the fluorescence vs. diameter with Ad^y was obtained using subroutine fit from Press et al. [46],

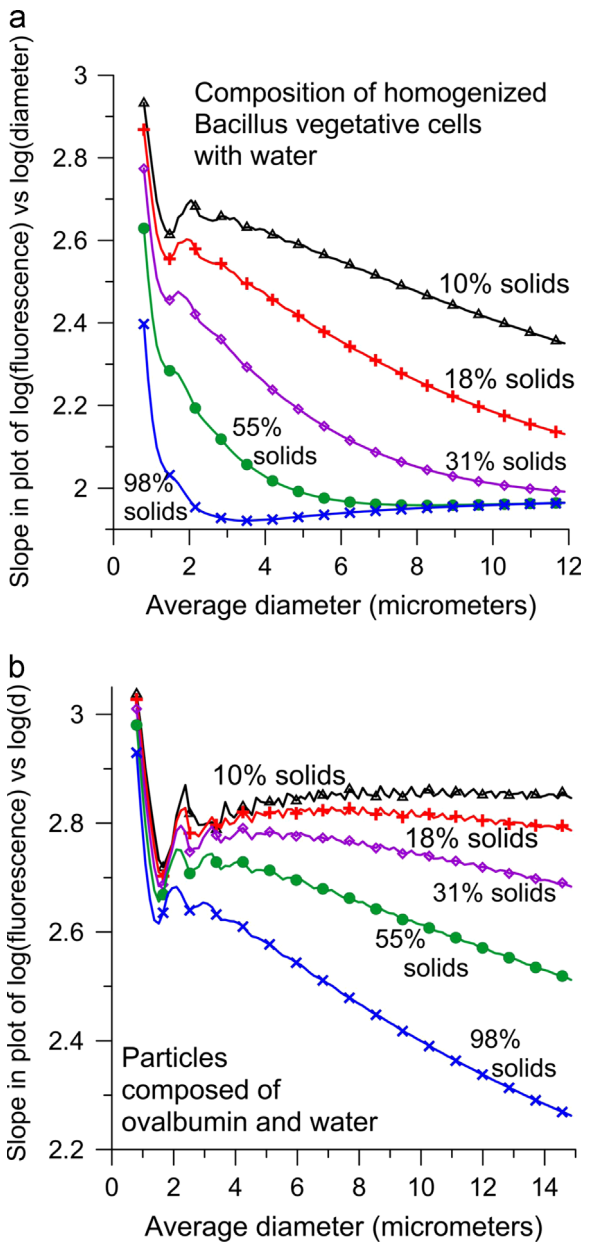

Fig. 8. Slope of $\log(C_F)$ vs. $\log(d)$ for particles with different fractions of water and solids. The solids have the composition in (a) of homogenized *Bacillus* vegetative cells as in Table 1, and in (b) of homogenized ovalbumin as in Table 1.

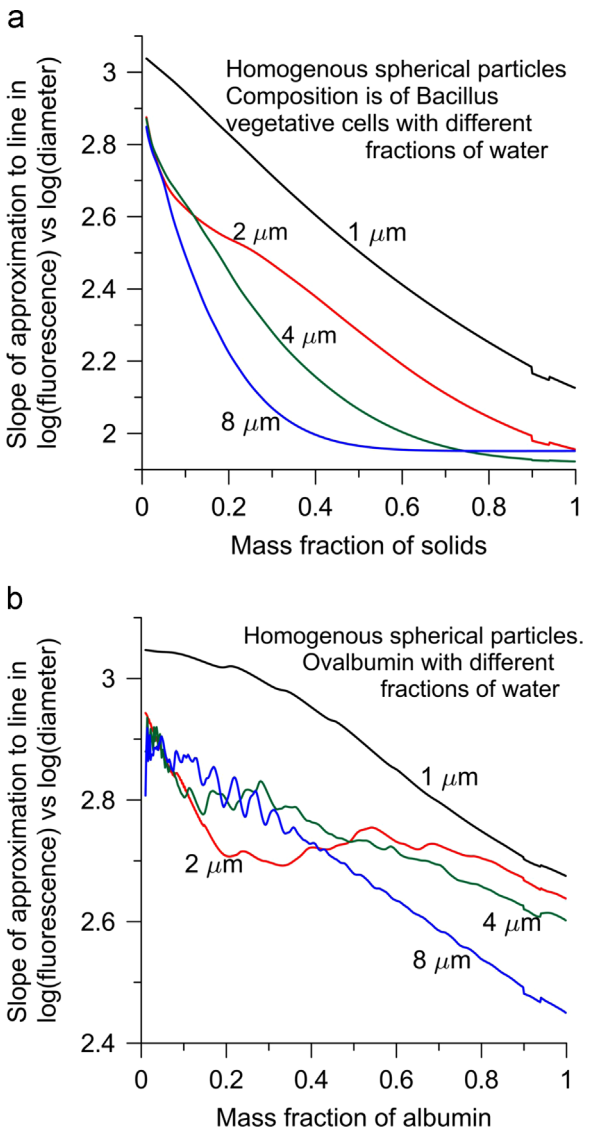

Fig. 9. Slope of $\log(C_F)$ vs. $\log(d)$ plotted vs. fraction of mass of solids for particles with different fractions of water and solids. The solids have the composition in (a) of homogenized *Bacillus* as in Table 1, and in (b) of ovalbumin.

with the log-fluorescence vs. log diameter for diameters between 0.4 and 8.6 μm.

The exponent y in Ad^y tends to decrease as the water content of a hygroscopic particle decreases. Also, the quality of the fit varies with fraction of solids. For the case of 98% solids, the fit is within approximately 5% between 0.8 and 10 μm. The closeness of this approximation is not so surprising given that in Fig. 8(a) the slopes for the case of 98% solids is within 12% of 2.0 for d between 1 and 12 μm. Even for the cases with higher water content in Fig. 10, the ratio of the calculated to the fit fluorescence is within 13% for diameters between approximately 1 and 10.5 μm. This result is more remarkable because in Fig. 8(a) the slopes in the slope vs. diameter plots vary by approximately 0.7 over the diameters from 1 to 10 μm for each of the other cases (18% and 31% solids).

3.7. *Possible use of Q vs d and C_F/d^y in estimating non-fluorescent content of particles*

Because the shape of the C_F vs. d curve is independent of R_F, comparisons of measured relative fluorescence with calculated C_F as in Figs. 1, 2 and 4 should not be over-interpreted to mean that the model parameters are close to the actual values. The shape of the C_F-vs.-d curve depends only on the total m, especially on m_i for the particles modeled here, and that shape is the only feature compared in Figs. 1, 2 and 4. Comparisons of the absolute

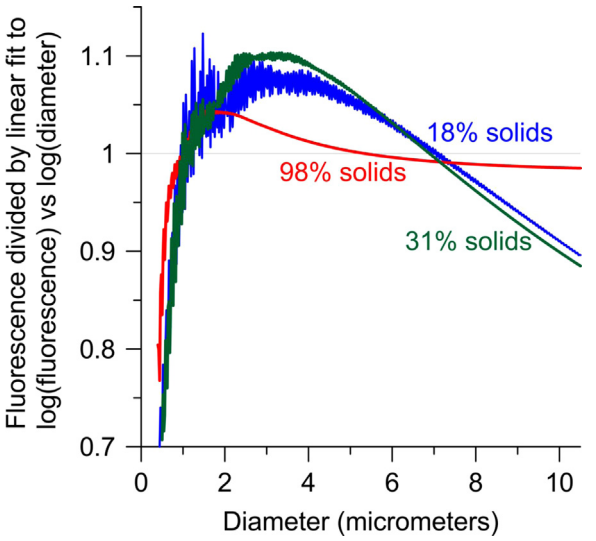

Fig. 10. Fluorescence-divided-by-Ad^y vs. diameter for the best fit combinations of A and y for spherical homogenous particles composed of water and solids where the solids have the composition of *Bacillus* vegetative cells shown in Table 1. For each fraction of solids, the A and y were fit to the calculated fluorescence. For 98% solids $y=1.97$; 31% solids $y=2.34$; 18% solids $y=2.53$.

magnitudes of the C_F-vs.-d or Q_F-vs.-d curves are essential for more complete and informative comparisons. Comparisons with absolute magnitudes of fluorescence are also needed to reach closure among all the measured quantities (concentrations, absorptivities, densities, fluorescence, particle diameter, etc.) and the modeled fluorescence. For example, if particles are assumed to be pure and dry but actually contain a large but unrecognized fraction of water or salt, then closure will not be possible (although some other errors might accidentally compensate these errors and cause even further problems).

If absolute C_F is measured for particles of various sizes, and the values are plotted as in Fig. 5, and the curve of Q_F vs. d reaches an asymptote, then m_i can be approximated by solving $(m_r-1)d/\delta=2$, using some reasonable estimate of m_r. Then the estimated m can be used to calculate the asymptotic value of Q_{abs}. This asymptotic Q_{abs} will probably be between 0.9 and 0.96 for any bioaerosol particle with enough absorption for Q_{abs} to approximately reach an asymptote. Then R_F is found as Q_F/Q_{abs}.

There is value in examining the shapes of these fluorescence vs. d curves whether the measured quantity is relative or absolute fluorescence. The variations in C_F with water content are clear in Figs. 3, 5, 6, and 8–10. These variations suggest the importance of estimating the content of water or other non-fluorescing materials when they might be in a sample. Consider particles generated by mixing a pure protein in water, aerosolizing the mixture, and then attempting to dry the droplets in air before their fluorescence is measured. Some proteins, such as albumins, are hygroscopic and dry relatively slowly. Figs. 5, 6 and 8–10 suggest that it should be possible to estimate the amount of water remaining in the particles at the time of measurement. The measured-fluorescence divided by $\pi d^2/4$ can be plotted vs. d and compared with calculations of fluorescence from particles of protein in water. These calculations would be made similarly to those in Figs. 5 and 6, but would be made using the parameters of the specific protein if known, or estimated if the amino acid content is known. The m that gives the best fit of the calculations to the measurements can be selected and used to estimate water content. Also, the measured relative fluorescence can be plotted vs. d in a log–log plot (as in Fig. 3), and the best fit slope (y) can be determined and compared with calculated values of y for different m (similar to those in Figs. 8 and 9). Such an approach can also be relevant for detecting other nonabsorbing materials such as salts or carbohydrates. Such materials can be relatively unimportant for many biological applications (e.g., growing more of a sample without contamination by other microbes), but can be very important for understanding the fluorescence of particles made from a sample. Or consider particles held for a sufficient time in air with a constant humidity so that their water content has come to equilibrium. This equilibrium depends upon the salt content and the types of protein or other biological material in the particle, as well as on the humidity. Calculations of Figures such as Figs. 5, 6 and 8–10 may be useful in understanding the growth and evaporation of particles.

There are limitations in attempting to use calculations of Q_F vs d or of F/d^y vs d, where F is the measured fluorescence, in estimating the content of water or other non-fluorescent materials. One is that instruments which measure single-particle fluorescence of aerosols flowing through them may collect different fractions of fluorescence from particles in different positions relative to the excitation beam and the collection optics. Another is that if the particles are generated by aerosolizing an aqueous solution or suspension, the larger droplets will take longer to dry and may have a higher fraction of water at the time of measurement. Also, when aerosolized droplets of solutions (of, e.g., proteins, carbohydrates and/or salts in water) are dried, the outer surface of the droplets may form a thin solid layer [47]. More complex shapes and internal distributions may also form depending upon the materials, diffusion rates, temperature, etc. [62,11]. For example, a solid or glassy layer may form at the droplet surface if the water leaves the particle surface more quickly by evaporation than water from inside the particle moves to the surface by diffusion. Such particles are not homogeneous. Fluorescent droplets and particles generated by using a nebulizer, or by persons who sneeze, cough [12] or flush a toilet [28], or by the breakup of water, may or may not be homogeneous, depending upon the initial size and composition of the droplets, as well as on the humidity and temperature of the surrounding air.

4. Summary and final comments

This paper uses a model similar to the one in [23,24] to calculate fluorescence vs. size for pure proteins and clean bacteria. Only the total fluorescence emitted in all directions is calculated. The model is applicable only to particles in which reabsorption of fluorescence within the particle is negligible. The particles studied in this paper (composed of pure proteins or clean bacteria, with varying amounts of

water) have negligible reabsorption for the sizes studied. As shown in Section 2, the modeling approach can be applied to particles composed of multiple homogeneous regions, to non-spherical particles, and to particles illuminated by complex waves, so long as methods to calculate the scattered and internal intensities of such particles are available. However, all the calculations presented here are for homogeneous spherical particles illuminated by plane waves. For the analyses done with these particles, we make the following observations.

The fluorescence cross section of a homogeneous particle can be calculated as the product of two terms, i.e., $C_F = C_{abs}\, R_F$, as discussed in (2.2.3), where R_F is the ratio of the energy-emitted-as-fluorescence to the energy-absorbed. The R_F is independent of the size and shape of the particle and depends only upon the absorbers and fluorophores in the material composing the particle. The absorption cross section, C_{abs}, depends on the particle size, shape, and the complex refractive index (m), especially m_i, but is independent of both the fluorescence quantum yields of the molecules in the particle and of the particular set of molecules that combined to give that m_i.

Calculated log–log plots of C_F vs. d can be approximately linear in certain size ranges, i.e., the approximation of $C_F = Ad^y$ can be adequate in those ranges where typically $2 \le y \le 3$ (Figs. 2, 3, 8–10). For the sizes of particles studied here, the y in Ad^y tends to decrease as the water content decreases (Figs. 3, 8 and 9). Also, for the bacteria and protein studied here, y decreases as d increases, for a given water content, until y is approximately 2, and then it remains approximately 2 for larger d. For example, Fig. 8(a) shows that the y for *Bacillus* mixed with 2%, 69% or 82% water decreases by approximately 0.74 as d increases from 1 to 10 μm. However, even with this significant variation in y, the plots in Fig. 10 of C_F-divided-by-Ad^y vs. d, for the best fit combinations of A and y, are within 13% for $1 < d < 10.5$ μm.

Plots of the particle fluorescence efficiency (Q_F) vs. d are also useful for visualizing and understanding the size dependence of C_F, and how y changes as d and/or m_i increase (Figs. 4–6). The shapes of the plots of Q_F in Figs. 4–6 vary as do plots of Q_{abs}. Because Q_F varies as C_F with its primary d-dependence (i.e., d^2) removed, the variations in Q_F vs. size (as a function of particle composition) as seen in Figs. 4–6, are more apparent than are the variations in C_F vs. size in Figs. 1–3. In comparisons of measured and calculated values, plots of Q_F vs. d (linear–linear) or of C_F/d^y vs. d (linear–linear) can emphasize outliers and deviations from the simplest approximations. On the other hand, plotting the measured fluorescence vs. size or log(fluorescence) vs. log(size), can make outlier points appear less significant than they do in plots of Q_F vs. d. When either Q_F or Q_{abs} is plotted vs. $m_i d$, or vs. d/δ, (δ = penetration depth), or vs. $m_i(m_r - 1)d$, the curves for the different m_i or δ tend to overlap (Fig. 6). These overlaps suggest an approximately general curve for the variation of Q_F with d and m, at least in the range of d and m appropriate for the biological compositions illustrated.

Comparisons of measured relative fluorescence with calculated C_F as in Figs. 1, 2 and 4 should not be over-interpreted to mean that the model parameters are close to the actual values. The shape of the C_F-vs.-d curve depends only on the total m, and, in the examples illustrated here, especially on m_i. Comparisons of the absolute magnitudes of the C_F-vs.-d curves appear to be essential for testing the assumptions about the molecules that make up the particles (their absorptivities, fluorescence quantum yields, and concentrations). Comparisons with absolute magnitudes of fluorescence are also needed to reach closure of the experiments with models and model parameters. However, the shapes of the measured fluorescence vs. size curves can help in testing assumptions about the content of water, salts, or other non-fluorescing molecules in particles. This is true even if the only measured quantity is the relative fluorescence intensity, especially if the optical properties of the non-water part of the particle is known. Figs. 3, 5, 6, and 8–10 illustrate how the calculated C_F varies with water content and suggest the use of figures such as these in estimating the particles' content of non-fluorescent materials, at least in cases where the composition of the biological part of the particles are known. Figs. 6 and 8–10 also suggest the use of figures such as these to extract ranges of m_i that are consistent with the measured data.

The results and concepts of this paper should be useful to developers and users of fluorescence-based instruments for single particle characterization. For example, this paper illustrates how important it is to understand the effects of humidity, and the particle's content of water and salt, on the fluorescence of particles of different sizes and compositions. Also, for example, the paper illustrates general shapes of the plots of Q_F vs. $m_i d$, or vs. d/δ which should be useful in fitting measured data on Q_F and d to appropriately shaped curves.

Acknowledgments

Supported by US Army Research Laboratory mission funds and the Defense Threat Reduction Agency (DTRA) Basic and Supporting Science Program (contract HDT RA1-10-C-0023).

References

[1] Agranovsky V, Ristovski ZD, Ayoko GA, Morawska L. Performance evaluation of the UVAPS in measuring biological aerosols: fluorescence spectra from NAD(P)H coenzymes and riboflavin. Aerosol Sci Technol 2003;38:354–64.
[2] Agrios GN. Plant pathology. 5th ed. Burlington, MA: Elsevier Academic; 2005.
[3] Arakawa ET, Tuminello PS, Khare BN, Milham ME. Optical properties of ovalbumin in 0.130–2.50 μm spectral region. Biopolymers 2001;62:122–8.
[4] Arakawa ET, Tuminello PS, Khare BN, Milham ME. Optical properties of *Erwinia herbicola* bacteria at 0.190–2.50 μm. Biopolymers 2003;72:391.
[5] Baldwin WW, Myer R, Powell N, Anderson E, Koch AL. Buoyant density of *Escherichia coli* is determined solely by the osmolarity of the culture medium. Arch Microbiol 1995;164:155–7.
[6] Barber PW, Hill SC. Light scattering by particles: computational methods. Singapore: World Scientific; 1990.
[7] Bennett BD, Yuan J, Kimball EH, Rabinowitz JD. Absolute quantitation of intracellular metabolite concentrations by an isotope ratio-based approach. Nat Protocols 2008;3:1299–311.
[8] Bennett BD, Kimball EH, Gao M, Osterhout R, van Dien SJ, Rabinowitz JD. Absolute metabolite concentrations and implied enzyme active site occupancy in *Escherichia coli*. Nat Chem Biol 2009;5:593–9.

[9] Berlman IB. Handbook of fluorescence spectra of aromatic molecules. 2nd ed. New York: Academic; 1971. p. 337.
[10] Bohren CF, Huffman DR. Absorption and scattering of light by small particles. New York: Wiley; 1983.
[11] Bones DL, Reid JP, Lienhard DM, Krieger UK. Comparing the mechanism of water condensation and evaporation in glassy aerosol. Proc Nat Acad Sci 2012;109:11613–8.
[12] Bourouiba L, Dehandschoewerker E, Bush JWM. Violent expiratory events: on coughing and sneezing. J Fluid Mech 2014;745:537–63.
[13] Boutou V, Favre C, Hill SC, Pan YL, Chang RK, Wolf JP. Backward enhanced emission from multiphoton processes in aerosols. Appl Phys B Lasers Optics 2002;75:145–52.
[14] Carrera M, Zandomeni RO, Sagripanti J-L. Wet and dry density of *Bacillus anthracis* and other *Bacillus* species. J Appl Microbiol 2008;105:68–77.
[15] Carslaw KS, Lee LA, Reddington CL, Pringle KJ, Rap A, Forster PM, et al. Large contribution of natural aerosols to uncertainty in indirect forcing. Nature 2013;503:67–71.
[16] Chew H, McNulty PJ, Kerker M. Model for Raman and fluorescence scattering by molecules embedded in small particles. Phys Rev A 1976;13:396–404.
[17] Christesen SD, Merrow CN, DeSha MS, Wong A, Wilson MW, Butler JC. Ultraviolet fluorescence lidar detection of bioaerosols. In: Proceedings of SPIE 2222, atmospheric propagation and remote sensing III, vol. 228; June 29, 1994. http://dx.doi.org/10.1117/12.177988.
[18] Delgado FF, Cermak N, Hecht VC, Son S, Li Y, Knudsen SM, et al. Intracellular water exchange for measuring the dry mass, water mass and changes in chemical composition of living cells. PLOS ONE 2013;8(7):1–11 (e67590).
[19] Despres VR, Huffman AJ, Burrows SM, Hoose C, Safatov A, Buryak G, et al. Primary biological particles in the atmosphere: a review. Tellus B 2012;64:15598.
[20] Eames I, Tang JW, Li Y, Wilson P. Airborne transmission of disease in hospitals. J R Soc Interface 2009;6:S697–702.
[21] Hairston PP, Ho J, Quant FR. Design of an instrument for real-time detection of bioaerosols using simultaneous measurement of particle aerodynamic size and intrinsic fluorescence. J Aerosol Sci 1997;28:471–82.
[22] Hill SC. Method for integrating the absorption cross section of spheres over wavelength or diameter. Appl Opt 2003;42:4381–8.
[23] Hill SC, Pan YL, Williamson C, Santarpia JL, Hill HH. Fluorescence of bioaerosols: mathematical model including primary fluorescing and absorbing molecules in bacteria. Opt Express 2013;21:22285–313.
[24] Hill SC, Doughty DC, Pan YL, Williamson C, Santarpia JL, Hill HH. Fluorescence of bioaerosols: mathematical model including primary fluorescing and absorbing molecules in bacteria: errata. Opt Express 2014;22:22817–9.
[25] Hill SC, Pinnick RG, Niles S, Fell NF, Pan YL, Bottiger J, et al. Fluorescence from air-borne microparticles: dependence on size, concentration of fluorophores, and illumination intensity. Appl Opt 2001;40:3005–13.
[26] Huffman JA, Sinha B, Garland RM, Snee-Pollmann A, Gunthe SS, Artaxo P, et al. Size distributions and temporal variations of biological aerosol particles in the Amazon rainforest characterized by microscopy and real-time UV-APS fluorescence techniques during AMAZE-08. Atmos Chem Phys 2012;12:11997–2019.
[27] Huffman JA, Treutlein B, Pöschl U. Fluorescent biological aerosol particle concentrations and size distributions measured with an Ultraviolet Aerodynamic Particle Sizer (UV-APS) in Central Europe. Atmos Chem Phys 2010;10:3215–33.
[28] Johnson D, Lynch R, Marchall C, Mead K, Hirst D. Aerosol generation by modern flush toilets. Aerosol Sci Technol 2013;47:1047–57.
[29] Jonsson P, Kullander F. Bioaerosol detection with fluorescence spectroscopy. In: Jonsson P, et al., editors. Bioaerosol detection technologies, integrated analytical systems. New York: Springer-Verlag; 2014. p. 111–41 (chapter 7).
[30] Kubitschek HE. Buoyant density variation during the cell cycle in microorganisms. Crit Rev Microbiol 1987;14:73–97.
[31] Kamihira M, Taniguchi M, Kobayashi T. Sterilization of microorganisms with supercritical carbon dioxide. Agric Biol Chem 1987;51:407–12.
[32] Kiselev D, Bonacina L, Wolf JP. A flash-lamp based device for fluorescence detection and identification of individual pollen grains. Rev Sci Instrum 2013;*84*(3):033302.
[33] Laflamme C, Simard J-R, Buteau S, Lahaie P, Nadeau D, Déry B, et al. Effect of growth media and washing on the spectral signatures of aerosolized biological stimulants. Appl Opt 2011;50:788–96.
[34] Lakowicz JR. Principles of fluorescence spectroscopy. 3rd ed. New York: Springer; 2006. pp. 58–59.
[35] Longworth JW. Luminescence of polypeptides and proteins. In: Steiner RF, Weinryb I, editors. Excited states of proteins and nucleic acids. New York: Plenum; 1971. p. 428–43 (chapter 6).
[36] Mishchenko MI, Tracis LD, Lacis AA. Scattering, absorption and emission of light by small particles. Cambridge: Cambridge University; 2002. 294 (chapter 6).
[37] Nelson DL, Cox MM. Lehninger principles of biochemistry. 5th ed. New York: Freeman; 2008. 76.
[38] O'Connor DJ, Healy DA, Sodeau JR. The on-line detection of biological particle emissions from selected agricultural materials using the WIBS-4 (Wavelength Integrated Bioaerosol Sensor) technique. Atmos Environ 2013;80:415–25.
[39] Pan Y-L, Hill SC, Wolf J-P, Holler S, Chang RK, Bottiger JR. Backward enhanced fluorescence from clusters of microspheres and particles of tryptophan. Appl Opt 2002;41:2994–9. (Fig. 3, p. 2997).
[40] Pan YL, Hill SC, Pinnick RG, Huang H, Bottiger JR, Chang RK. Fluorescence spectra of atmospheric aerosol particles measured using one or two excitation wavelengths: comparison of classification schemes employing different emission and scattering results. Opt Express 2010;18:12436–57.
[41] Pan YL, Hill SC, Santarpia JL, Brinkley K, Sickler T, Coleman M, et al. Spectrally-resolved fluorescence cross sections of aerosolized biological live agents and simulants using five excitation wavelengths in a BSL-3 laboratory. Opt Express 2014;22:865–8189.
[42] Pan YL, Pinnick RG, Hill SC, Rosen JM, Chang RK. Single-particle laser-induced-fluorescence spectra of biological and other organic-carbon aerosols in the atmosphere: measurements at New Haven, CT and Las Cruces, NM, USA. J Geophys Res 2007;112:D24S19.
[43] Pan YL, Santarpia JL, Ratnesar-Shumate S, Corson E, Eshbaugh J, Hill SC, et al. Effects of ozone and relative humidity on fluorescence spectra of octapeptide bioaerosol particles. J Quant Spectrosc Radiat Transf 2014;133:538–50.
[44] Penndorf RB. An approximation method to the Mie theory for colloidal spheres. J Phys Chem 1958;62:1537–42.
[45] Pohlker C, Huffman JA, Poschl U. Autofluorescence of atmospheric bioaerosols – fluorescent biomolecules and potential interferences. Atmos Meas Tech 2012;5:37–71.
[46] Press WH, Teukolsky SA, Vetterling WT, Flannery BP. Numerical recipes in Fortran. 2nd ed. Cambridge: Cambridge; 1992. pp. 655–660.
[47] Putkiranta M, Manninen A, Rostedt A, Saarela J, Sorvajarvi T, Marjamaki M, et al. Fluorescence properties of biochemicals in dry NaCl composite aerosol particles and in solution. Appl Phys B 2010;99:841–51.
[48] Robinson NH, Allan JD, Huffman JA, Kaye PH, Foot VE, Gallagher M. Cluster analysis of WIBS single-particle bioaerosols data. Atmos Meas Tech 2013;6:337–47.
[49] Saari SE, Putrikanta MJ, Keskinen J. Fluorescence spectroscopy of atmospherically relevant bacterial and fungal spores and potential interferences. Atmos Environ 2013;71:202–9.
[50] Saari SE, Reponen T, Keskinen J. Performance of two fluorescence-based real-time bioaerosol detectors: bioscout vs. UVAPS. Aerosol Sci Technol 2014;48:371–8.
[51] Santarpia JL, Pan YL, Hill SC, Baker N, Cottrell B, McKee L, et al. Changes in fluorescence spectra of bioaerosols exposed to ozone in a laboratory reaction chamber to simulate atmospheric aging. Opt Express 2012;20:29867–81.
[52] Sirotkin AM, Komissarov IA, Khadiullina AV. Hydration of proteins: excess partial volumes of water and protein. J Phys Chem B 2012;116:4098–105 (Fig. 1 (A) and (B).
[53] Sivaprakasam V, Huston A, Scotto C, Eversole JD. Multiple UV wavelength excitation of bioaerosols. Opt Express 2004;12:4457–66.
[54] Sivaprakasam V, Lin HB, Huston AL, Eversole JD. Spectral characterization of biological aerosol particles using two-wavelength excited laser-induced fluorescence and elastic scattering measurements. Opt Express 2011;19:6191–208.
[55] Steinberg IZ. Long-range nonradiative transfer of electronic excitation energy in proteins and polypeptides. Annu Rev Biochem 1971;40:83–114.
[56] Stocker TF, Qin D, et al. Technical summary. In: Stocker TF, Qin D, Plattner G-K, Tignor M, Allen SK, Boschung J, Nauels A, Xia Y, Bex V, Midgley PM, editors. Climate change 2013: the physical science basis. Contribution of working group I to the fifth assessment report of the intergovernmental panel on climate change, 114. Cambridge, United Kingdom and New York, NY, USA: Cambridge University Press; 2013. p. 53–7.
[57] Sugimoto N, Huang Z, Nishizawa T, Matsui I, Tatarov Boyan. Fluorescence from atmospheric aerosols observed with a multi-channel lidar spectrometer. Opt Express 2012;20:20800–7.

[58] Sun J, Ariya PA. Atmospheric organic and bio-aerosols as cloud condensation nuclei (CCN): a review. Atmos Environ 2006;40(5):795.
[59] Taketani F, Kanaya Y, Nakamura T, Koizumi K, Moteki N, Takegawa N. Measurement of fluorescence spectra from atmospheric single submicron particle using laser-induced fluorescence technique. J Aerosol Sci 2013;58:1–8.
[60] Toprak E, Schnaiter M. Fluorescent biological aerosol particles measured with the Waveband Integrated Bioaerosol Sensor WIBS-4: laboratory tests combined with a one year field study. Atmos Chem Phys 2013;13:225–43.
[61] Van de Hulst HC. Light scattering by small particles. New York: Wiley; 1957 (Dover, 1981).
[62] Vehring R. Pharmaceutical particle engineering via spray drying. Pharm Res 2008;25:999–1022.
[63] Velesco N, Kaiser T, Schweiger G. Computation of the internal field of a large spherical particle by use of the geometrical-optics approximation. Appl Opt 1997;36:8724–8.
[64] Velesco N, Schweiger G. Geometrical optics calculation of inelastic scattering on large particles. Appl Opt 1999;38:1046–52.
[65] Vesilovsky I, Griaznov V, Kolgotin A, Whiteman DN. Angle- and size-dependent characteristics of incoherent Raman and fluorescent scattering by microspheres. 2. Numerical simulation. Appl Opt 2002;41:5783–91.
[66] Yankofsky SA, Levin Z, Bertold T, Sandlerman N. Some basic characteristics of bacterial freezing nuclei. J Appl Meteorol 1981;20:1013–9.
[67] Yu ITS, Li Y, Wong TW, Tam W, Chan AT, Lee JHW, et al. Evidence of airborne transmission of the Severe Acute Respiratory Syndrome Virus. N Engl J Med 2004;350:1731–9.